(4)

AFGL-TR-88-0138

APPLICATION AND EVALUATION OF A DIFFERENTIAL INVERSION TECHNIQUE FOR REMOTE TEMPERATURE SENSING

Robert G. Hohlfeld
Ronald F. Wachtmann
James C. Kilian

Creative Optics, Inc.
32 Wildwood Drive
Bedford, MA 01730

Final Report
July 1986-May 1988

30 June 1988

APPROVED FOR PUBLIC RELEASE; DISTRIBUTION UNLIMITED

AIR FORCE GEOPHYSICS LABORATORY
AIR FORCE SYSTEMS COMMAND
UNITED STATES AIR FORCE
HANSCOM AFB, MASSACHUSETTS 01731

"This technical report has been reviewed and is approved for publication"

DR. JEAN I.F. KING
Contract Manager

FOR THE COMMANDER

ROBERT A. McCLATCHEY, Director
Atmospheric Sciences Division

This report has been reviewed by the ESD Public Affairs Office (PA) and is releasable to the National Technical Information Service (NTIS).

Qualified requestors may obtain additional copies from the Defense Technical Information Center. All others should apply to the National Technical Information Service.

If your address has changed, or if you wish to be removed from the mailing list, or if the addressee is no longer employed by your organization, please notify AFGL/DAA, Hanscom AFB, MA 01731. This will assist us in maintaining a current mailing list.

Do not return copies of this report unless contractual obligations or notices on a specific document requires that it be returned.

REPORT DOCUMENTATION PAGE

1a. REPORT SECURITY CLASSIFICATION: UNCLASSIFIED	1b. RESTRICTIVE MARKINGS:
2a. SECURITY CLASSIFICATION AUTHORITY: N/A	3. DISTRIBUTION/AVAILABILITY OF REPORT: Approved for public release; distribution unlimited
2b. DECLASSIFICATION/DOWNGRADING SCHEDULE: N/A	
4. PERFORMING ORGANIZATION REPORT NUMBER(S): COI-SR-24	5. MONITORING ORGANIZATION REPORT NUMBER(S): AFGL-TR-88-0138
6a. NAME OF PERFORMING ORGANIZATION: Creative Optics, Inc. / 6b. OFFICE SYMBOL (If applicable):	7a. NAME OF MONITORING ORGANIZATION: Air Force Geophysics Laboratory
6c. ADDRESS (City, State and ZIP Code): 32 Wildwood Drive, Bedford. MA 01730	7b. ADDRESS (City, State and ZIP Code): Hanscom AFB, Massachusetts 01731-5000
8a. NAME OF FUNDING/SPONSORING ORGANIZATION: U.S. Air Force Geophysics Laboratory / 8b. OFFICE SYMBOL (If applicable): LY	9. PROCUREMENT INSTRUMENT IDENTIFICATION NUMBER: F19628-86-C-0167
8c. ADDRESS (City, State and ZIP Code): Hanscom Air Force Base, MA 01731	10. SOURCE OF FUNDING NOS.

PROGRAM ELEMENT NO.	PROJECT NO.	TASK NO.	WORK UNIT NO
62101F	ILIR	6D	AA

11. TITLE (Include Security Classification) (cont. on reverse)
Application and Evaluation of a Differential

12. PERSONAL AUTHOR(S)
Robert G. Hohlfeld, Ronald F. Wachtmann*, James C. Kilian

13a. TYPE OF REPORT	13b. TIME COVERED	14. DATE OF REPORT (Yr., Mo., Day)	15. PAGE COUNT
Final	FROM JUL 86 TO MAY 88	1988 June 30	42

16. SUPPLEMENTARY NOTATION
*ST Systems Corp., 109 Massachusetts Ave., Lexington, MA
This research was supported by the Inhouse Laboratory Independent Research Fund.

17. COSATI CODES		
FIELD	GROUP	SUB. GR.

18. SUBJECT TERMS (Continue on reverse if necessary and identify by block number)
Differential Inversion, Remote Sensing, Atmospheric Temperature Profiles

19. ABSTRACT (Continue on reverse if necessary and identify by block number)

Abstract

A new theoretical approach is developed for remote temperature sensing based on Laplace transform techniques applied to the radiative transfer equation. This approach allows calculation of the atmospheric temperature profile based on measurements of the upwelling radiance and its derivatives. A detailed numerical study of this technique is carried out and the technique is applied to measurements of the upwelling radiance taken with a balloon-borne Fourier transform spectrometer (SCRIBE), and to data from the Tiros Operational Vertical Sounder (TOVS). Limitations of the technique arising from experimental errors, truncation errors, roundoff errors, and other causes are discussed.

20. DISTRIBUTION/AVAILABILITY OF ABSTRACT	21. ABSTRACT SECURITY CLASSIFICATION
UNCLASSIFIED/UNLIMITED ☒ SAME AS RPT. ☐ DTIC USERS ☐	UNCLASSIFIED

22a. NAME OF RESPONSIBLE INDIVIDUAL	22b. TELEPHONE NUMBER (Include Area Code)	22c. OFFICE SYMBOL
Dr. Jean King	617/377-2976	AFGL/LY

DD FORM 1473, 83 APR EDITION OF 1 JAN 73 IS OBSOLETE.

11. Title (cont.)

Inversion Technique for Remote Temperature Sensing.

ACKNOWLEDGEMENTS

The following individuals were helpful to the authors in the course of this research. We wish particularly to acknowledge technical discussions with Dr. Jean I. F. King of the U.S. Air Force Geophysics Laboratory Division of Atmospheric Sciences (who was the Contracting Officer's Technical Representative). Dr. King provided great insight into the problem and the development of an analytical approach to the data analysis. Dr. Vincent Falcone, also of the AFGL Division of Atmospheric Sciences, provided important scientific insights regarding atmospheric radiance data anad analysis. Mr. W. O. Gallery of OptiMetrics, Inc. provided the raw SCRIBE data along with a quality analysis of the data. Mr. M. Chalfant of NOAA/NESDIS provided the TOVS filter data. Mr. M. Goldberg of ST Systems Corporation provided the TOVS radiance data. Finally the generous assistance of Mr. J. Chetwynd of the AFGL Optical Physics Division was essential to the successful application of the FASCODE model in this work. The authors thank Dr. John F. Ebersole of Creative Optics, Inc. who was the Program Manager.

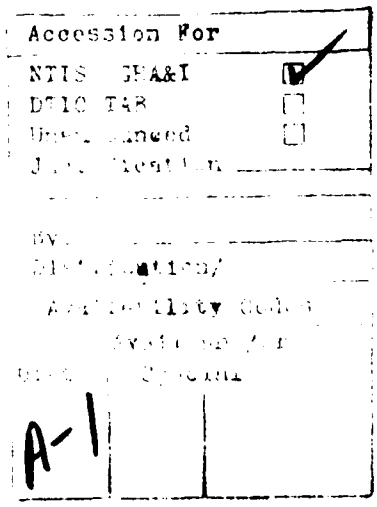

Table of Contents

EXECUTIVE SUMMARY

In this research we have successfully carried out an implementation of the differential inversion algorithm developed by Dr. Jean I. F. King of the Air Force Geophysics Laboratory. This algorithm is an exciting advance in the methodology of atmospheric temperature sensing because it allows the computation of atmospheric temperature profiles from upwelling radiances and their derivatives in a computationally effective fashion.

The primary problem in any implementation of the differential inversion is the control of numerical instability. A portion of this instability is intrinsic to the differential inversion algorithm because it is based upon Laplace transform techniques; the rest is due to use of finite difference schemes to evaluate numerical derivatives (which are sensitive to the presence of experimental and other errors). We have learned how to control these numerical instabilities as a result of studies carried out on synthetic radiance data which characterized the properties of the differential inversion algorithm on a controlled data set.

We then applied the differential algorithm to upwelling radiance data from SCRIBE and TOVS. Owing to the difficulties in calibration and the noise level in the SCRIBE data, inversion errors on the order of 20 K were obtained. However, inversion of TOVS data involved errors on the order of only 2 K.

We have demonstrated that the differential inversion algorithm may be successfully employed to invert radiance data to obtain atmospheric temperatures. Our work suggests several profitable avenues for research to improve the accuracy and utility of the differential inversion algorithm, both through improvements in the algorithm itself and throught developments in temperature sounder instrumentation.

1 INTRODUCTION

Satellite observations provide the only practical means of obtaining temperature profiles in the atmosphere over large geographic areas (especially over oceans) and over long periods of time. This implies that the development of new and computationally effective algorithms for measuring atmospheric temperature profiles from satellite data is a significant and important task.

The measurable quantity most accessible to satellite observations is the infrared upwelling radiance. Most typically this is measured at wavelength $\sim$ 15 μm, near the atmospheric CO_2 absorption band. Different spectral regions in this wavelength region become optically thick at different heights in the atmosphere, and so the upwelling infrared radiance in those wavelength intervals contains, at least in principle, information about the Planck function at different heights in the atmosphere. On this basis, one should be able to determine a temperature profile of the atmosphere using measurements of the upwelling infrared radiance.

In practice, we must solve the radiative transfer equation for the Planck function over this spectral interval, a Fredholm integral equation of the first kind. Since we are dealing with an integral equation, we must cope with problems of non-uniqueness of the solution obtained. This is a problem of practical importance because the range of plausible solutions of the transfer equation (within limits imposed by the accuracy of the experimental data) cover an unacceptably large range of temperatures.

A number of workers have approached this problem with techniques designed to obtain the "true" temperature profile (or at least a pragmatically useful profile) by a variety of methods, most of which require some *a priori* assumptions such as the assumption of an initial temperature profile. Application of relaxation techniques (Chahine 1970, 1972; Smith 1970; Yeh, Vonder Haar, and Liou 1985) requires the selection of an initial temperature profile to commence an iterative process. Application of the method of Backus and Gilbert (Conrath 1972) requires the assumption of a reference temperature profile in order to evaluate radiative transfer kernels.

Other relevant work has been undertaken (Twomey 1970) to delineate the limits in information content of solutions of the radiative transfer equation. In this vein, Fourier analysis of the radiative transfer equation (Gautier and Revah 1975) allows treatment of the temperature profile as a band-limited spectrum.

In this paper we consider a new approach to this problem based on Laplace transform theory (King 1983, 1985). This technique uses the upwelling radiance measurements and their logarithmic pressure derivatives to construct an atmospheric temperature profile. This method has the particular theoretical attraction of assuming no *a priori* information about the temperature profile beyond the fact that it is reason-

ably smooth (*i.e.* analytic). Our numerical studies and simulations using this algorithm have investigated the viability of this approach and indicated some of its sensitivities to truncation error, roundoff error, experimental uncertainty, and other noise processes. This differential inversion technique has been applied to a set of Fourier transform spectrometer data in the 15 μm spectral region and to a sample of data from the NOAA TIROS Operational Vertical Sounder (TOVS). On the basis of these studies, we shall evaluate this technique and discuss instrument designs optimally suited to its application.

2 THEORY OF DIFFERENTIAL INVERSION

2.1 General Theory

In this section we develop the theory of differential inversion techniques as applied to the detemination of atmospheric temperature profiles on the basis of the infrared upwelling radiance. This infrared upwelling radiance might be measured by a satellite or a balloon-borne spectrometer at high altitudes. For sake of completeness, we shall develop the theory of differential inversion in some detail. Our treatment follows the development of this subject by King (1985).

Radiative transfer theory relates the upwelling thermal radiance of an atmosphere to an integral transform over pressure of the Planck intensity $\mathcal{B}(p)$ and a weight function $\mathcal{W}(p/\bar{p})$. The weight function is determined by the detailed line character of the sampled interval, effectively sampling that height of the atmosphere at which the optical depth in that spectral interval is near unity. Therefore, the radiance of the wavelength channel whose weight function peaks at $p = \bar{p}$ is given by

$$\mathcal{R}(\bar{p}) = \int_0^\infty \mathcal{B}(p)\mathcal{W}(p/\bar{p})\, dp/p. \tag{1}$$

A change of independent variable into logarithmic pressure units, with modified functions $\mathcal{B}(p) = B(-\ln p)$, $\mathcal{R}(\bar{p}) = R(-\ln \bar{p})$, and $\mathcal{W}(p) = W(\ln p)$ converts the expression for the upwelling radiance (1), into a convolution integral,

$$R(\varsigma) = \int_{-\infty}^{\infty} B(z)W(\varsigma - z)\, dz \equiv B * W, \tag{2}$$

where $z = -\ln p$, and $\varsigma = -\ln \bar{p}$ are height-like variables. This convolution integral form motivates the application of Laplace transform theory to solve for the Planck function and equivalently for the temperature. Application of the bilateral Laplace transform using the Faltung theorem results in

$$r(s) = b(s)w(-s), \tag{3}$$

with r, b, and w, the Laplace transforms of R, B, and W, respectively, and s the Laplace transform variable. It will be seen that the bilateral transform of the weight function

$$w(-s) = \int_{-\infty}^{\infty} e^{-sz}W(z)\, dz = \int_0^\infty p^{-s}\mathcal{W}(p)\, dp/p \equiv \Omega(1-s), \tag{4}$$

may be viewed as a generalized Γ function. This is significant for practical applications of the theory in which it may be desirable to approximate atmospheric weight functions in some convenient fashion.

We shall use expansion techniques to solve for the Planck function as a function of height. Proceed by expanding the reciprocal of the Ω function in a MacLaurin series,

$$\frac{1}{\Omega(1-s)} = \sum_{k=0}^{\infty} \lambda_k (-s)^k, \tag{5}$$

in which the coefficients λ_k are given by

$$\lambda_k = \frac{[w^{-1}(0)]^{(k)}}{k!}. \tag{6}$$

The expansion coefficients are thus seen to involve the kth derivative with respect to the transform variable s of the bilateral weight transform, evaluated at $s = 0$. We may now express the Laplace transform of the Planck function in terms of a series involving the λ_k's and the transform of the radiance,

$$b(s) = \sum_{k=0}^{\infty} \lambda_k s^k r(s). \tag{7}$$

Taking the inverse Laplace transform of (7) then yields the differential inversion formula we seek,

$$B(z) = \sum_{k=0}^{\infty} \lambda_k D^{(k)} R(\zeta) = R(\zeta) + \lambda_1 R'(\zeta) + \lambda_2 R''(\zeta) + \ldots \tag{8}$$

This formula has been derived formally for Laplace transform inversion by Widder (1971).

2.2 Differential Inversion Coefficients and Generalized Weight Functions

Calculation of the Planck function profile depends on the inversion coefficients which are determined by the particular form of the weight function. Determination of detailed atmospheric weight functions over a range of frequencies is a computationally demanding task. It is frequently desirable to work with an approximate form which has most of the relevant features of actual atmospheric weight functions and the advantage of computational tractability.

We shall now develop closed-form expressions and numerical values using such an approximation to the weight functions. Define the generalized exponential weight function,

$$\mathcal{W}_m(P) = \frac{m^m}{\Gamma(m+1)} P \exp(-mP^{1/m}), \tag{9}$$

where $P = p/\bar{p}$, with $\bar{p}$ the pressure at which the weight function achieves its maximum. The generalized exponential weight function satisfies the normalization requirements,

$$\int_0^{\infty} \mathcal{W}_m \, dp/p = \int_{-\infty}^{\infty} W_m(z) \, dz = 1. \tag{10}$$

The parameter m adjusts the effective width of the generalized exponential weight function, smaller values of m, "sharpen" the weight function, *i.e.* decrease its effective width. It should be noted that the particular choices of $m = 1$ and $m = 1/2$ correspond to the Goody-statistical and the Elsasser band models, respectively.

The bilateral Laplace transform of the weight function follows (see eq (4)) as

$$\int_{-\infty}^{\infty} e^{-sz} W_m(z)\, dz = \int_0^{\infty} p^{-s} \mathcal{W}_m(p)\, dp/p = \Gamma_m(1-s), \tag{11}$$

where we have defined the mth order Γ function as

$$\Gamma_m(s+1) = \frac{\Gamma[m(s+1)]}{m^{ms}\Gamma(m)}. \tag{12}$$

The evaluation of the coefficients λ_k, as can be seen from Equations (4), (6), and (12), involves the derivatives of the Γ function. The first derivative is related to the digamma or ψ function

$$\psi(s) = \Gamma'(s)/\Gamma(s), \tag{13}$$

and its higher derivatives the polygamma functions

$$\psi^{(k)}(s) = \frac{d^{k+1}}{ds^{k+1}} \ln \Gamma(s). \tag{14}$$

Closed form expressions for the inversion coefficients λ_k $(k = 0, 1, \ldots, 6)$ as a function of the weight parameter m are given in King (1985). For integer and half-integer argument, the polygamma functions are expressible in terms of the Riemann zeta functions.

Calculation of inversion coefficients, given for some special cases in Tables 1 and 2, is straightforward but tedious. Note that as the weight function becomes increasingly concentrated, corresponding to smaller m, that all λ_k's tend to zero for $k > 1$, while $\lambda_1(m \to 0) \to -1$. This implies that even for a delta-type weight function, there is a shift between the Planck intensity and the radiance profile extrema, *i.e.* $p_{min} \neq \bar{p}_{min}$, where $\mathcal{B}_{min} = \mathcal{B}(p_{min})$, and $\mathcal{R}_{min} = \mathcal{R}(\bar{p}_{min})$. Furthermore, the extent to which the odd coefficients differ from zero is a measure of the asymmetry of the weight function. Therefore,

$$\lambda_i \neq 0 \quad (i = 1, 3, 5, \ldots) \Rightarrow W(-z) \neq W(z).$$

2.3 Expected Limitations of Differential Inversion Techniques

This theoretical discussion of the differential inversion technique allows us to anticipate some of the difficulties that might be encountered in implementing this method

Table 1: Inversion coefficients for generalized exponential weight function with $m = 1$, taken from (King 1985).

λ_0	+1.0
λ_1	-0.5772156649
λ_2	-0.6558780715
λ_3	+0.0420026350
λ_4	+0.1665386114
λ_5	+0.0421977346
λ_6	-0.0096219715
λ_7	-0.0072189432
λ_8	-0.0011651676
λ_9	+0.0002152417
λ_{10}	+0.0001280503
λ_{11}	+0.0000201349
λ_{12}	-0.0000012505

Table 2: Differential inversion coefficients for representative general exponential weight functions.

	Delta function $m = 0$	Strongly peaked $m = 0.1$	Elsasser $m = 0.5$	Statistical $m = 1$	Strong clustering $m = 4$
λ_0	+1.0	+1.0	+1.0	+1.0	+1.0
λ_1	-1.0	-0.8121169848	-0.6351814227	-0.5772156649	-0.5207067709
λ_2	0.0	-0.1773994973	-0.4151225552	-0.6558780715	-2.1350158750
λ_3	0.0	-0.9119348444	-0.0014993282	+0.0420026350	0.3050207816
λ_4	0.0	+0.0004253445	+0.0416237314	+0.1665386114	2.2390138114
λ_5	0.0	+0.0001167500	+0.0104035581	+0.0421977346	+0.4628141296

for obtaining atmospheric temperature profiles. First of all, it is apparent that we will obtain some level of truncation error owing to the necessity of terminating the series in Equation (8) after some finite number of terms. In practice, the number of terms at which we will have to terminate this series will depend on the reliability of our measured radiances and their derivatives, and as is well known, numerical differentiation of experimental data corrupted by noise is at best a chancy business. It would be very surprising if more than the first few derivatives of radiance data from actual measurements were reliable. Therefore, we will investigate the extent to which this is of importance in the differential inversion algorithm.

Practical difficulties also arise in the determination of the weight functions. The weight functions may either be determined by regression techniques or determined by differentiation of atmospheric transmittance profiles. Therefore, there is some uncertainty associated with the weight function, and with the location of its maximum, $\bar{p}$. This is especially true when the weight function is obtained by differentiation of the transmittance, where problems in accurately obtaining numerical derivatives may be important. The uncertainty in the weight functions is also reflected in the evaluation of the λ coefficients which depend on moments of the weight function.

In addition to these practical limitations, a more fundamental difficulty must be considered. Evaluation of inverse Laplace transforms, as is required in differential inversion, is known to be a numerically unstable process (Widder 1971), compared to the situation in Fourier inversion, where demonstrably stable and accurate algorithms exist. The reason for this numerical instability arises ultimately from the fundamental different character of the exponential function for real and imaginary arguments. For real arguments, x, e^{-x} is a smooth and monotonic function from $x = 0$ to $x = \infty$; and for imaginary arguments the exponential becomes oscillatory, maintaining its average amplitude for all x. It is apparent then if we want the Laplace transform, $\int_0^\infty e^{-sx} f(x)\, dx$, to show some response to values of x around $x = 100$, say, then s must be small enough that e^{-sx} is appreciably different from zero. Say that we need $s \approx 0.01$; now the derivative of e^{-sx} is $-se^{-sx}$, and since s is small, then so is its derivative and so the function e^{-sx} changes only slowly around $x = 100$. This implies that we will have considerable difficulty in resolving features in the function $f(x)$ around $x = 100$, *i.e.* distinguishing $f(100)$ from say $f(99)$ or $f(101)$. Also rapid fluctuations in $f(x)$ in the neighborhood of $x = 100$ will give only a small change in $\int_0^\infty e^{-sx} f(x)\, dx$. These considerations show that kernels with smooth behavior can yield unstable solutions, *i.e.* in terms of the physical variables of our particular problem, small changes in the upwelling radiance can yield large changes in the inferred temperature profile one obtains as a result of differential inversion computations. Control of this fundamental numerical instability is of fundamental importance in the successful implementation of the differential inversion algorithm.

3 NUMERICAL IMPLEMENTATION OF THE DIFFERENTIAL INVERSION ALGORITHM

Performing a differential inversion for the determination of temperature as a function of altitude, utilizing the infinite series derived in the previous section, requires the computation of the inversion coefficients, λ_i, and the derivatives (out to nth order) of the radiance with respect to $\varsigma = -\ln(\bar{p})$.

The derivatives of the radiance were estimated by a centered finite-difference technique (*cf.* Chapra and Canale 1985). This was carried out by constructing a one dimensional grid around each point for which the derivative was to be evaluated, and then applying the finite differences to those points. To lowest order, the truncation error of this technique falls off as $O(h^2)$, where h is the spacing between grid points.

The lowest order version of the finite difference requires a total of four grid points in order to obtain derivatives to fourth order at a single data point. Therefore, in the particular problem addressed here, an atmospheric radiance profile is decomposed into an $5N \times 2$ matrix consisting of points corresponding to $\ln(\bar{p})$ and radiance over N vertically distributed layers of the atmosphere, and four grid points symmetrically located about each of the N layers each also consisting of a value of both radiance and $\ln(\bar{p})$.

The grid point spacing in $\ln(p)$ was initially taken as constant for the synthetic data studies. However for real data this is not always feasible. Therefore, another variation in the centered finite-difference technique that accomodates variable grid point spacing must be used.

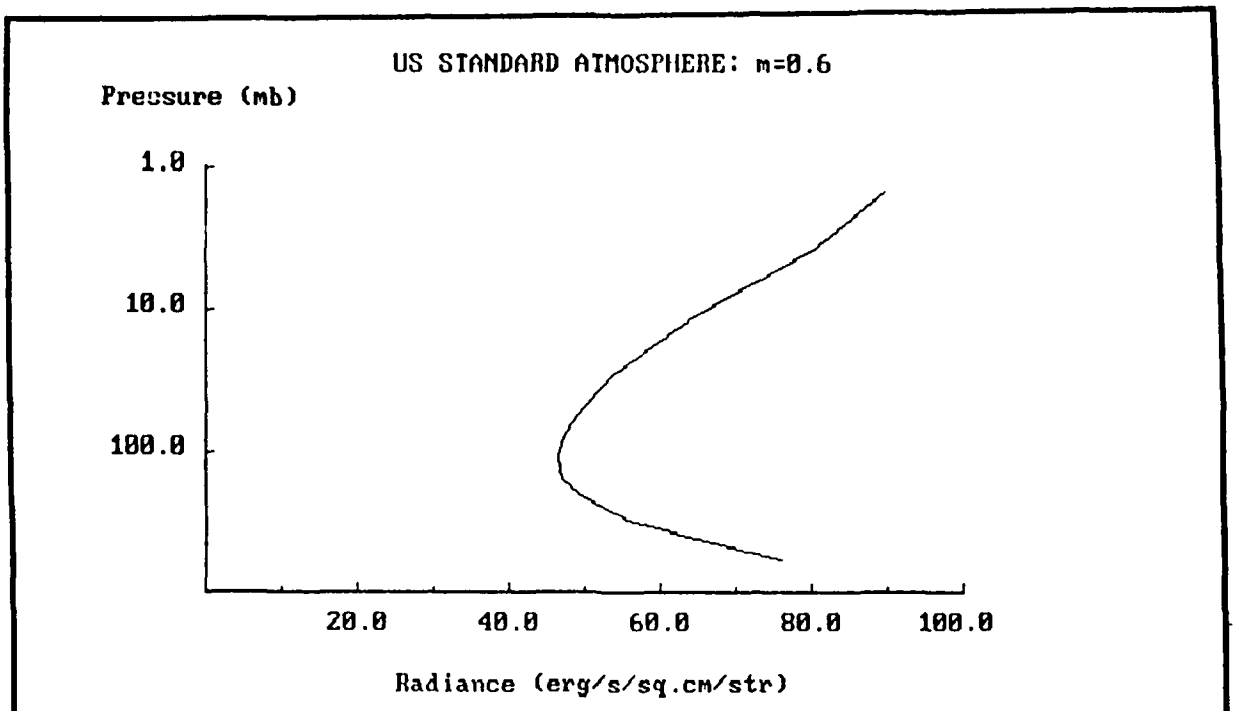

Figure 1: Synthetic radiance profile computed for a generalized exponential weight function with $m = 0.6$. Radiances were calculated using the U.S. Standard Atmosphere.

4 APPLICATION TO SYNTHETIC DATA

In order to ascertain the strengths and weaknesses of the King inversion equation, the implementation described above was applied to synthetic radiance data. An evaluation of the impact of truncation of Equation (8) and of numerical errors on the accuracy and stability of the differential inversion technique is made possible by examination of the differential inversion independently of the presence of experimental noise in the data.

The radiance profile was computed from the transfer equation using the generalized exponential in equation (9) as a weighting function. Atmospheric temperature and pressure information specified as the U.S. Standard Atmosphere (Champion *et al.* 1985). A constant wavenumber was used throughout the synthetic data study. In order to account for the contribution of the earth's surface to the upwelling radiance a surface term,

$$R_0 = B_0\Big[1 - \int_0^{p_0} W(p/\bar{p})\, dp/p\Big]$$

was included. Figure 1 shows the output radiance profile from such a synthetic radiance profile calculation.

In order to accommodate points in the atmosphere near the surface of the earth, for which some of the associated grid points may actually fall below the surface of the earth, the surface term allows the radiance profile to be extrapolated by treating the earth as a semi-infinite, isothermal component of the atmosphere.

The accuracy of the synthetic radiance profile is limited by numerical error in the computations. All calculations were performed in double-precision. Initially, the transfer equation was integrated using Simpson's rule; however, gross round-off errors led to the adoption of Romberg's method of integration (Press *et al.* 1986). Again, the error level was much higher than expected, but nonetheless, orders of magnitude better than was obtained with Simpson's method. The error, primarily roundoff from the integration, is on the order of ± 0.01 ergs/sec/cm^2/ster/cm^{-1} for the synthetic radiance profile. This number is typical, but does not apply to all weight functions. Later, in the discussion it will be shown that generalized exponential weighting functions with $m = 0.1$ and $m = 1.0$ produce different inversion accuracies which result from the propagation of the error discussed here.

The radiance profile is fed directly into the inversion routine where the derivatives are obtained. Values of m of 0.1, 0.5, and 1.0 for generalized exponential weight functions were used to cover a range of possible atmospheric weight functions. Inversion coefficients for these m values were taken from King (1985).

The comparison of the resulting temperatures with those arising directly from the U.S. Standard Atmosphere are expressed as a simple difference

$$\Delta T = T_0 - T_1,$$

and an *rms* fluctuation of ΔT about zero.

$$\Delta T_{rms} = \sqrt{\sum (\Delta T)^2 / N}.$$

The spacing between points in the finite difference grid h, proved to be a parameter to which the inversion is quite sensitive. Figure 2 illustrates the accuracy of the inversion relative to the stepsize h. The graph implies that the grid about a single point must be large on the scale of the entire atmosphere in order to minimize the *rms* fluctuations of ΔT about zero. The problem arises from the fact that the synthetic radiance profile is not error free. To illustrate, define

$$g(x_i, h) = (f(x_{i+1}) - f(x_{i-1}))/2h$$

where $f(x)$ is a differentiable (order n) function, and x_{i+1} and x_{i-1} are points equally spaced on either side of a point x_i. For brevity, $f_{i+1} = f(x_{i+1})$, $f_{i-1} = f(x_{i-1})$, and $f_i = f(x_i)$.

Define a function $K(x)$, which is constructed from some point-by-point representation of $f(x)$ (*i.e.* data), then

$$K(x_i) = f(x_i) \pm \delta_i,$$

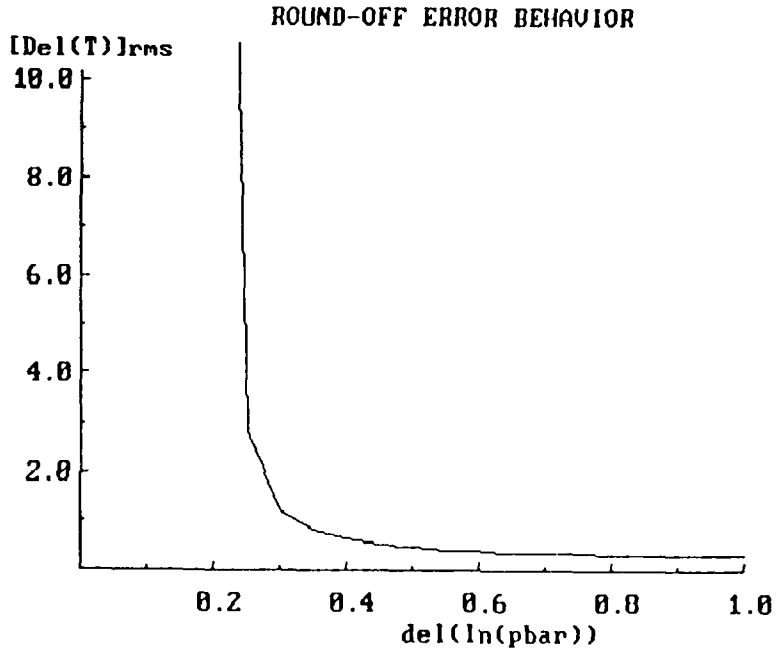

Figure 2: Calculation of total numerical error on the basis of synthetic radiance calculations as a function of stepsize h for numerical differentiation. For stepsizes less than approximately 0.35 the total numerical error begins to diverge.

where δ_i is the degradation contained in the construction of $K(x)$, and is defined as

$$\delta_i = |K(x_i) - f(x_i)|.$$

Define a function

$$G(h) = (K(x_{i+1}) - K(x_{i-1}))/2h$$

where x_{i+1} and x_{i-1} are as defined above. This may be rewritten as

$$G(h) = g(h) \pm \sigma,$$

with

$$\sigma_{min} \leq \sigma \leq \sigma_{max},$$

where

$$\sigma = |\delta_{i+1} \pm \delta_{i-1}|/2h,$$

$$\sigma_{max} = (|\delta_{i+1}| + |\delta_{i-1}|)/2h$$

and

$$\sigma_{min} = 0.$$

Thus,

$$\lim_{h \to 0} G(h) = df/dx \pm \sigma.$$

It can be seen that σ may become very large in the limit $h \to 0$, because the δ's can be nearly independent of h. Consider a specific example, let all the δ's equal 0.01, then Table 3 gives values of σ_{max} for estimates of derivatives of $K(x)$ (*i.e.* $f(x)$) at $h = 0.001$, 0.01, 0.1, and 1.0.

Figures 3 through 5 show the inversion results on synthetic data with various m values for the generalized exponential weighting functions. Point spacing for each case is $h = 0.35$ for $m = 0.1$, $h = 0.70$ for $m = 0.5$, and $h = 1.1$ for $m = 1.0$. Note that the fluctuation about zero increases at high pressure. With the stepsizes indicated above, the remaining error in the inversion stems, most likely, from the truncation of Equation (8), after the fifth term.

The results just given indicate that noise inherent in data will be critical to the application of this inversion technique. In real data, one typically does not have the

Table 3: Total error in the estimation of derivatives as a function of stepsize h.

	$h = 0.001$	$h = 0.01$	$h = 0.1$	$h = 1.0$
1st deriv.	10.0	1.0	0.1	0.01
2nd deriv.	4.0×10^4	400.0	4.0	0.04
3rd deriv.	3.0×10^7	3.0×10^4	30.0	0.3
4th deriv.	2.0×10^{12}	2.0×10^8	2.0×10^3	1.6

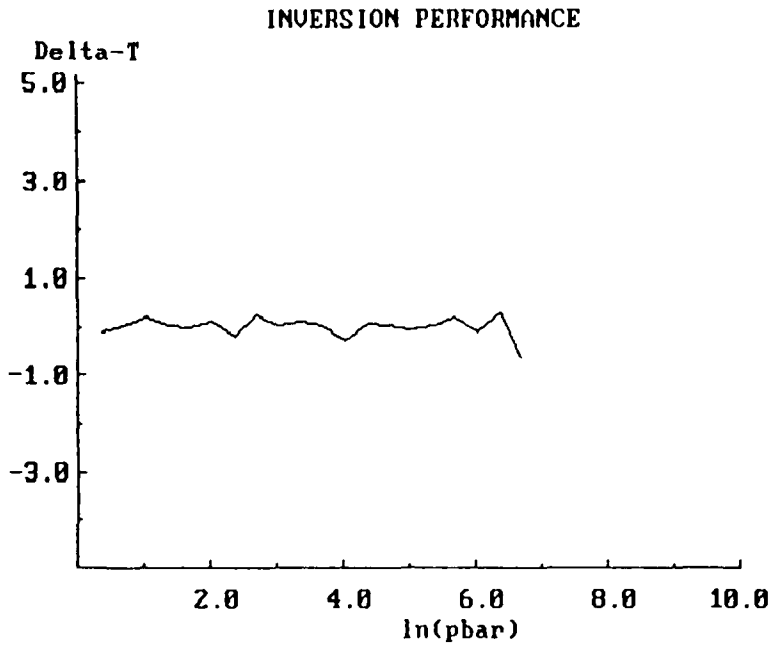

Figure 3: Errors in differential inversion of synthetic radiance data as a function of pressure with $h = 0.35$ and $m = 0.1$.

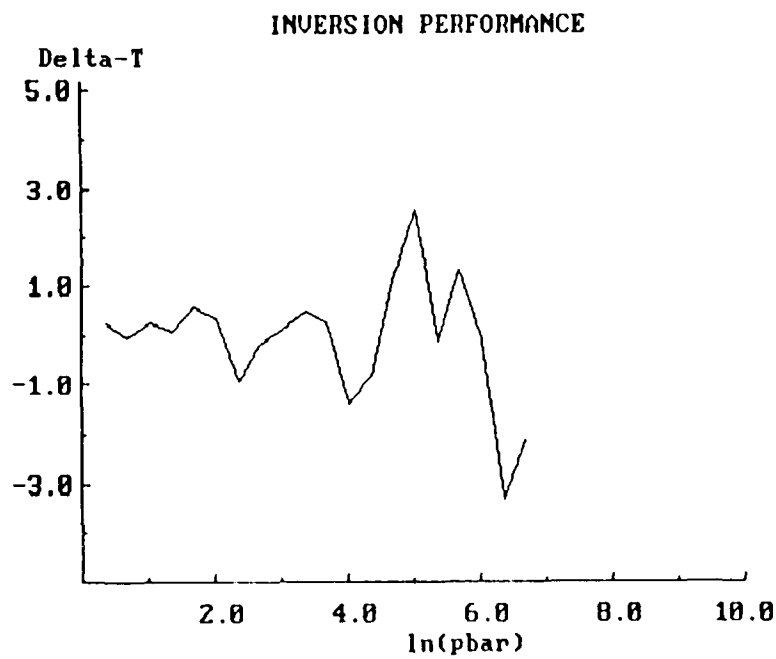

Figure 4: Errors in differential inversion of synthetic radiance data as a function of pressure with $h = 0.70$ and $m = 0.5$.

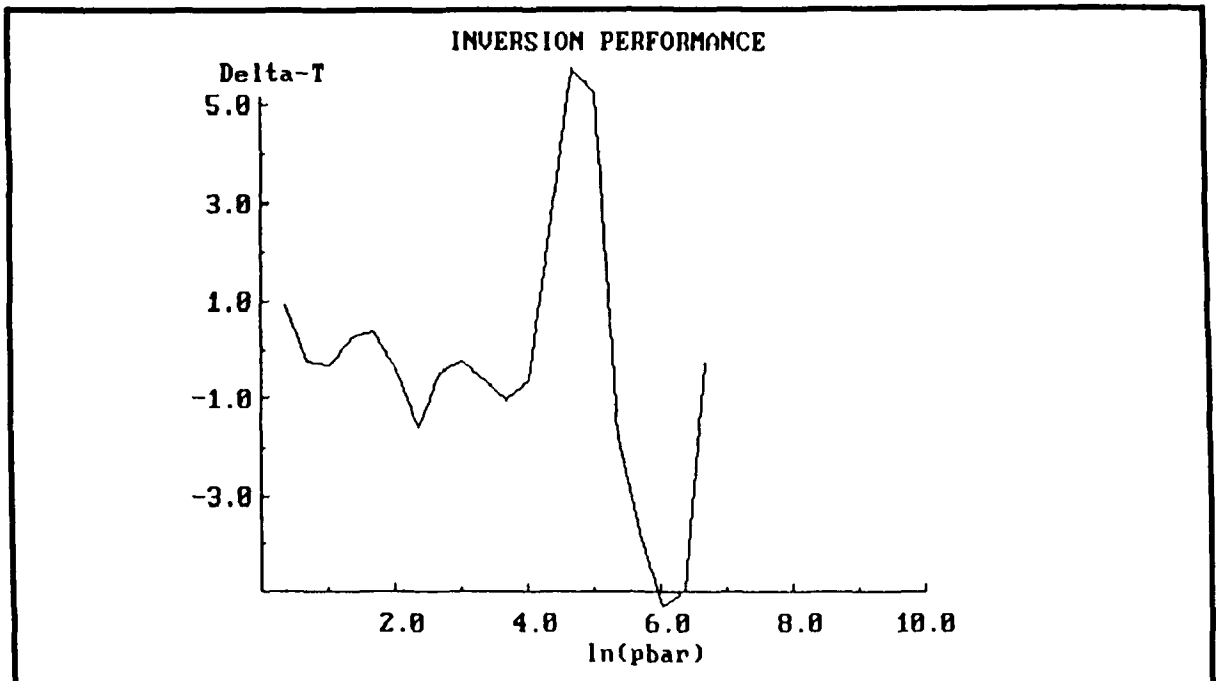

Figure 5: Errors in differential inversion of synthetic radiance data as a function of pressure with $h = 1.0$ and $m = 1.0$.

luxury of positioning data points for optimization of a single application of that data. In order to gain some insight into the behavior of King's equation in the presence of noise, random gaussian noise with selectable amplitude was added to the synthetic data.

Radiance profiles with grid spacings of $h = 0.35$ and $h = 0.9$ were generated using a generalized exponential weighting function with $m = 0.6$. The results of King's differential inversion technique are given in Figures 6 and 7. Again, the critical role of the grid point spacing, h, is apparent upon comparison of these two curves.

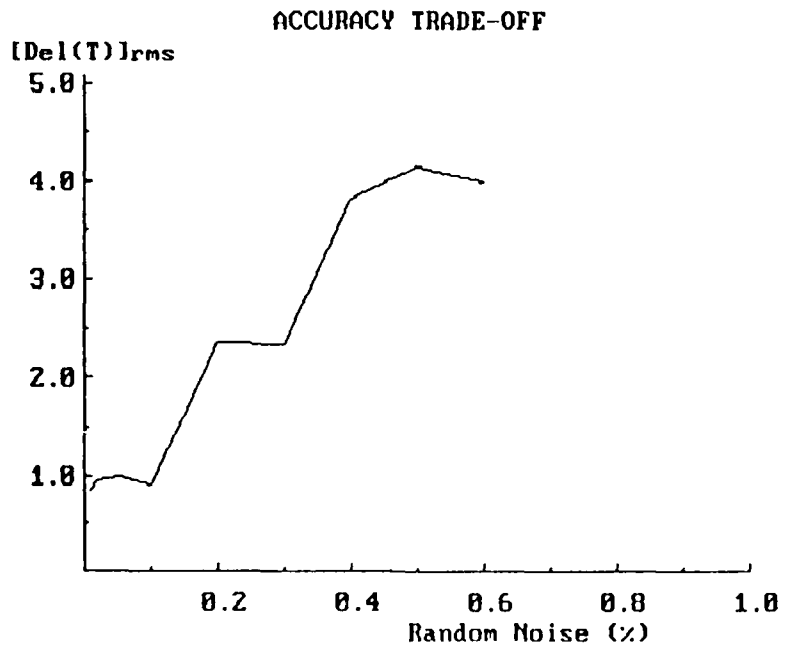

Figure 6: Accuracy of differential inversion in the presence of Gaussian distributed random noise in the radiance data. Values of $m = 0.6$ and $h = 0.35$ were used.

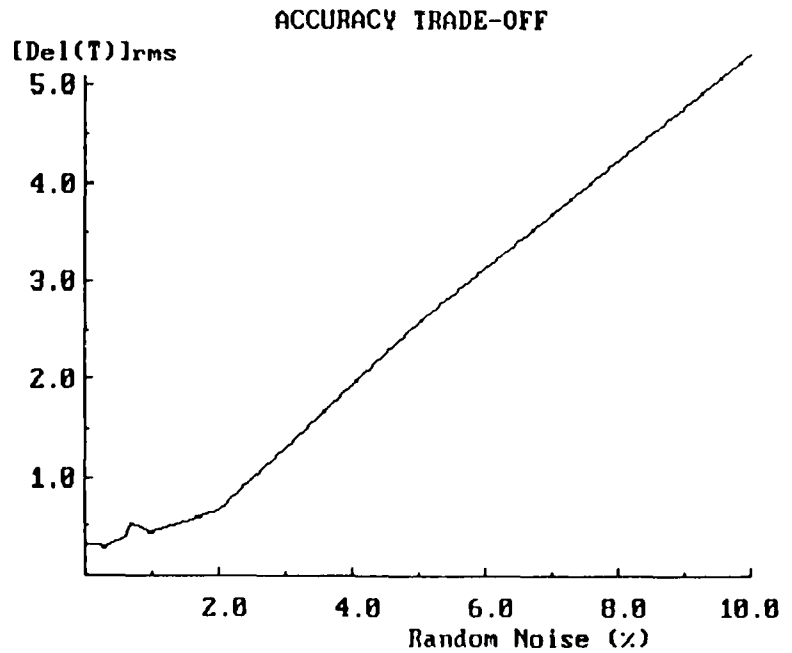

Figure 7: Accuracy of differential inversion in the presence of Gaussian distributed random noise in the radiance data. Values of $m = 0.6$ and $h = 0.95$ were used.

5 APPLICATION TO MEASURED RADIANCES

5.1 General Discussion

A basic purpose of this work was to apply the differential inversion technique to measured atmospheric radiance data. This particular aspect of the work had the following objectives:

1. To define a practical methodology for application of the algorithm to atmospheric measurements.
2. To evaluate the performance of the algorithm in temperature inferencing from measurements. Specifically, we sought the sensitivity of the algorithm to such factors as spectral resolution of the measurements, the properties of atmospheric weight functions, and noise in the radiance measurements.
3. To provide insight into the kinds of atmospheric radiance measurements that would support operational temperature inferencing by the differential inversion technique.

Two sources of measured data were identified for this application. The first is the Air Force Geophysics Laboratory's Stratospheric Cryogenic Interferometric Experiment (SCRIBE). The second is the NOAA TIROS Operational Vertical Sounder (TOVS). In section 5.2 we discuss the application of the algorithm to the SCRIBE data. Section 5.3 discusses the application to the TOVS data.

5.2 The SCRIBE Application

The SCRIBE program was established by the Air Force Geophysics Laboratory for the primary purpose of measuring straospheric emisssions at high spectral resolution from balloon altitudes (Vanasse 1981; Gallery *et al.* 1987). Two flights of the SCRIBE (23 Oct 83 and 5 Jul 84) at Holloman AFB, NM, were identified as potential data sources for this study.

The SCRIBE is a cryogenically cooled Fourier transform spectrometer configured to provide radiance data for the spectral interval from 500 cm^{-1} to 2500 cm^{-1}. The spectral resolution of the measurements is about 0.06 cm^{-1}. The instrument may be stepped through four different viewing directions ranging from 7.5° above the horizon to the nadir. Spectral scans are repeated at approximately 30 second intervals (Murcray *et al.* 1985, 1984; Vanasse 1981). Data are transmitted from the balloon to a ground

Table 4: Principal parameters describing the two scans of SCRIBE data from the 23 October 1983 flight that were used to test the application of the differential inversion algorithm. The two scans are identified as SP830V3 and SP830V1, respectively. (Gallery *et al.* 1987)

Parameter	Scan SP830V3	Scan SP830W1
Minutes after launch	100.8	104.0
Altitude above mean sea level (km)	30.36	30.67
Zenith view angle (degrees)	180.0	180.0
Radiosonde temperature at flight altitude (K)	232	233
667 cm^{-1} brightness temperature (K)	225	225
800 cm^{-1} brightness temperature (k)	270	272

recording station during the balloon flight. Reduction of the digital interferograms into radiance spectra requires several processing steps. This processing was accomplished at the University of Massachusetts for the data which we used in our application (Sakai 1985).

Gallery *et al.* (1987) carefully examined the October 1983 data for radiometric and spectroscopic calibration, noise level and comparison of the spectral radiance distributions to expected distributions calculated from the AFGL FASCOD2 model. The *rms* noise level of these data has been estimated to be of the order of approximately 2×10^{-7} watts/(cm ^{2} sr cm^{-1}). In addition, the spectral registration of the data is known to be displaced from its true position by a constant multiplicative factor. Based on these results we identified two downlooking scans from the 23 October 83 flight that were suitable for application of the differential inversion algorithm. The two scans were taken about three minutes apart. Table 4 presents pertinent details of the two scans. In order to improve the spectral registration of the data, we have analyzed the data in reference to the very accurately known positions of the strong absorption lines of carbon dioxide in the spectral region from 600 to 1200 cm^{-1}.

Figure 8 shows a full resolution plot of the SCRIBE radiances from ScanSP830V3 in the spectral region at 675 – 681 cm^{-1}. In this opaque portion of the spectrum, the radiance profile represents the temperature structure immediately below balloon altitude, where the temperature increased with height (see Figure 10). Here the peaks in the radiance profile represent peak absorption positions corresponding to the strong lines. The positions of the four strongest absorption lines in this region are represented

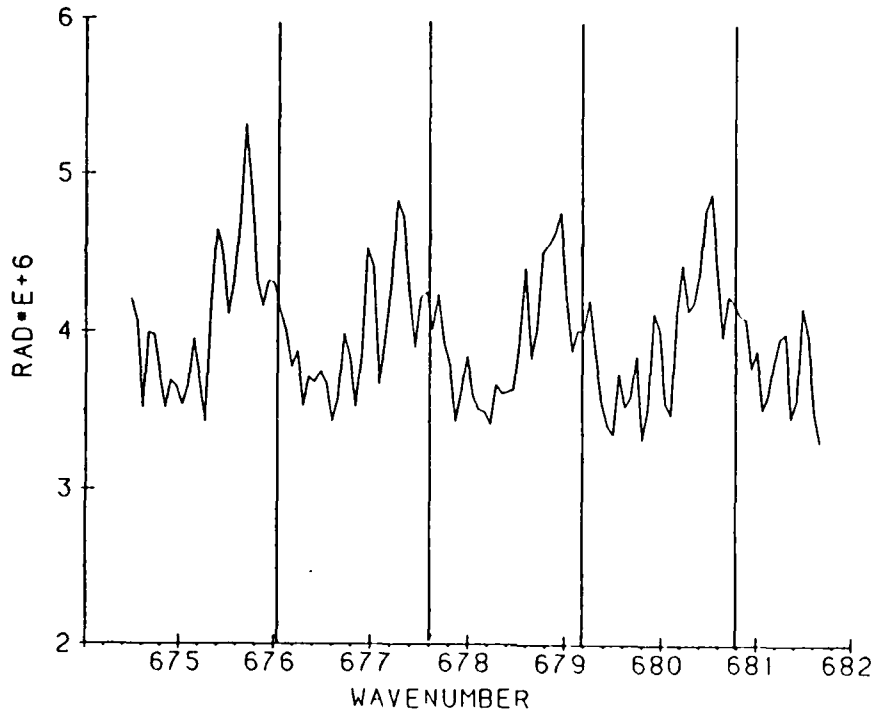

Figure 8: Radiance spectrum from SCRIBE Scan 830V3 on 23 July 1983. The vertical lines indicate positions of strong carbon dioxide lines at 676.0196, 677.6010, 679.1856, and 680.7733 cm^{-1} respectively. Radiance units are $erg/cm^2 sec\ ster\ cm^{-1}$ scaled by a factor of 10^6.

by the vertical lines.

Figure 9 shows a similar plot in the spectral region at $705 - 712\ cm^{-1}$. Here, the atmosphere is more transparent and the radiant energy originates in a layer where the temperature decreases with height above ground. Hence, the strong line positions are located in the radiance minima in the spectrum. The strong line positions are also represented on this plot by vertical lines.

The extrema in the radiance spectrum are shifted from line positions by about $0.3\ cm^{-1}$. We computed a correction factor K for both scans such that $\nu' = K\nu$, where ν is the reported spectral position of each data point and ν' is the corrected spectral position. The value of K for Scan 830V3 was 1.00049 and 1.00050 for the second scan, indicating consistency in its value.

Fluctuations of K about its mean correspond to a variation in corrected spectral position of about 0.03 to $0.05\ cm^{-1}$. This is the same order of magnitude as the resolution of the data. Hence, variations in the individual estimates of K may be ascribed largely to resolution limitations in the measured radiances.

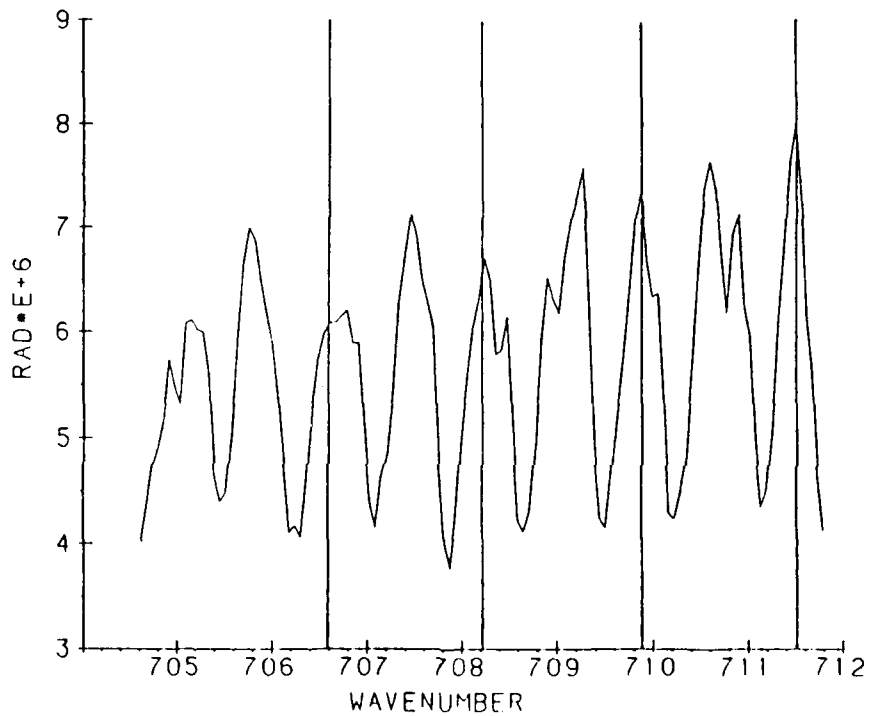

Figure 9: Radiance spectrum from Scan 830V3 in the spectral region from 705 to 712 cm^{-1}. The vertical lines indicate positions of strong carbon dioxide lines at 706.5763, 708.2121, 709.8503, and 711.4909 cm^{-1} respectively.

Selection of a suitable set of spectral bands required for such a radiance profile was not a straightforward process. We had no a priori knowledge of the specific distribution of weight functions for a specified set of bands. Furthermore, we wanted to generate band radiance sets at several different bandwidths in order to evaluate the effects of spectral resolution on algorithm performance.

5.2.1 FASCODE Calculations

The AFGL FASCODE Model was used to generate high resolution transmittance profiles for the atmospheric column from balloon altitude to the earth's surface for the period of the 23 Oct 83 flight of the SCRIBE. The FASCODE model is described in detail in Clough *et al.* (1986), Clough *et al.* (1981) and Smith *et al.* (1978). FASCODE is a highly developed program for fast, efficient computation of accurate, high-resolution atmospheric transmission profiles. The model assumes a layered atmosphere. The calculations are based on an optimum sampling at each layer from the AFGL line compilation (Rothman 1981).

We input to the model the temperature and moisture profiles reported in a Holloman radiosonde observation taken at the approximate time of the balloon flight. The profile is shown in Figure 10. Only the temperature and the moisture profiles were specified in the input profile. US Standard Atmosphere default profiles were used for the other constituent gases represented in the model.

In order to achieve as much detail as possible in the transmittance profile we generated profiles at 60 levels, the maximum permitted by FASCODE, between balloon altitude and the ground. This resulted in 0.5 km vertical spacing between transmittance levels.

The transmittance profiles used in the radiance band selection were constructed from the 0.006 cm^{-1} transmittances by using the FASCODE filter option. We constructed square filter functions with 101 data points per filter. Five sets of filters were used to generate the five transmittance files at the five different values of spectral resolution. Each transmission profile was differentiated to obtain the weight functions $(\partial\tau/\partial \ln p)$ and to locate the pressure level of the weight function peak.

5.2.2 Calculation of Weight Functions and Inversion Coefficients

Weight functions were calculated from the transmittances calculated from FASCODE by numerical differentiation. A centered divided difference calculation modified for unevenly spaced data was used to obtain the numerical derivatives. It was determined that inaccuracies in the FASCODE transmittances prevented calculation of physically meaningful

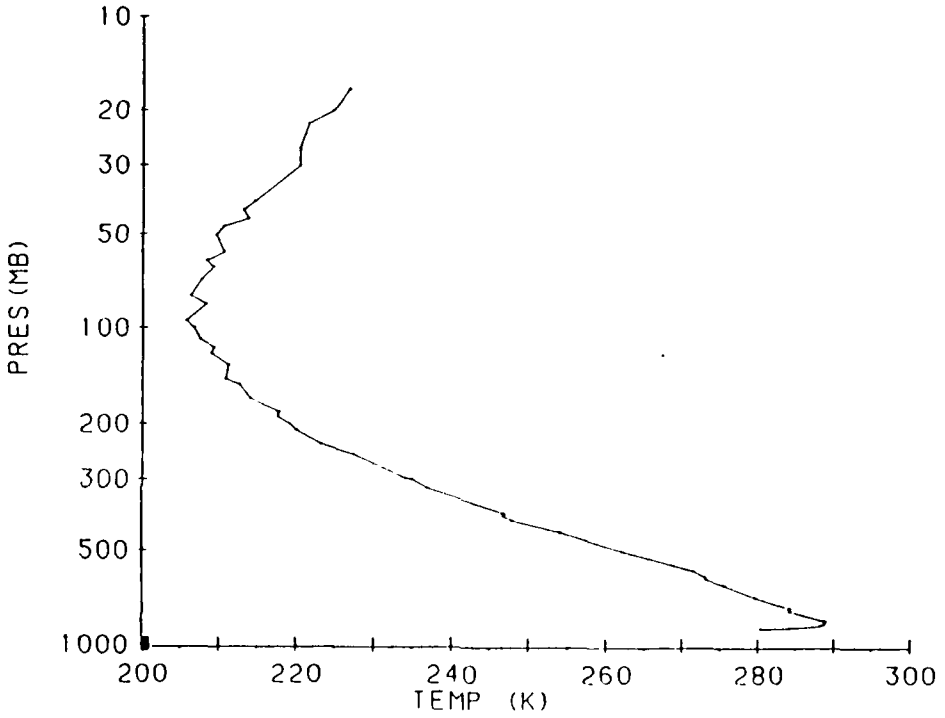

Figure 10: The atmospheric temperature profile from the Holloman rawinsonde observation of 23 July 1983. The approximate time of the rawindonde was 0700 MST (1400 GMT).

weight functions throughout the range of atmospheric pressures observed with SCRIBE. The problem is especially severe for the small transmittances at the low pressure end of the FASCODE pressure grid (see Appendix A).

These inaccuracies in FASCODE transmittances cause oscillations in the calculated weight functions with a period of two pressure grid intervals. The amplitude of the oscillations may be as great as the value of the nominal peak of the weight function. Since we expect that the weight functions must be smooth functions of the pressure, the weight functions obtained by numerical differentiation of FASCODE transmittances are unsuitable for use in differential inversion. The problem is especially severe for the evaluation of the inversion coefficients, λ_i, which involve determination of the *ith* moment of the weight function with respect to pressure. Numerical errors at the edge of the pressure grid particularly corrupt the evaluation of λ_i for large values of i.

Since these oscillations of the weight functions calculated from FASCODE transmittances are nonphysical, we are justified in using a fitting procedure based upon the physically reasonable portion of the weight function curves obtained by numerical differentiation. We fitted generalized exponential weight functions (see eq. (9)) to these FASCODE derived weight functions. Typically five points from the low pressure end of the FASCODE pressure grid were discarded in the process of constructing the generalized exponential fit. Given the m value resulting from the generalized exponential fit, values of λ_i may be obtained either numerically (using a Romberg integration algorithm) or on the basis of analytic formulae.

5.2.3 Description of SCRIBE Band Radiance Sets

Two spectral scans from the 23 October 83 flight were selected for application of the differential inversion algorithm. Their identifications are SP830V3 and SP830W1 respectively. Table 5 summarizes the band radiance sets that were constructed from these two scans. The radiance sets were constructed by convolution of rectangular filter functions with the full resolution spectra. Each set contained anywhere from 7 to 70 radiances depending on the spectral resolution and the number of radiances assigned for evaluation of derivatives at the $\bar{p}$ level. The number of $\bar{p}$ levels in each set varied from 1 to 10.

The sets are ordered as follows:

1. by the two scans, SP830V3 and SP830W1.
2. by spectral resolution; the values of resolution are indicated for each set.
3. by two differing values of nominal vertical spacing, *i.e.*, by the coarseness of the finite difference gird used in numerical evaluation of the derivatives.

Table 5: Summary of SCRIBE Band Radiance Sets

Scan	File name	Spectral Resolution cm^{-1}	Nominal h	Number of radiances *per* $\bar{p}$	Number $\bar{p}$ levels
SP830V3	BNRD21	1.0	0.20 to 0.25	7	10
	BNRD22	2.0			5
	BNRD23	0.1			10
	BNRD24	5.0			4
	BNRD25	10.0			4
	CNRD21	1.0	0.35 to 0.40	7	4
	CNRD22	2.0			4
	CNRD23	0.1			6
	CNRD24	5.0			2
	CNRD25	10.0			1
	DNRD21	1.0	0.35 to 0.40	5	2
	DNRD22	2.0			2
	DNRD23	0.1			2
	DNRD24	5.0			2
	DNRD25	10.0			2
SP830W1	ENRD21	1.0	0.20 to 0.25	7	10
	ENRD22	2.0			5
	ENRD23	0.1			10
	ENRD24	5.0			4
	ENRD25	10.0			4
	FNRD21	1.0	0.35 to 0.40	7	4
	FNRD22	2.0			4
	FNRD23	0.1			6
	FNRD24	5.0			2
	FNRD25	10.0			1
	GNRD21	1.0	0.35 to 0.40	5	2
	GNRD22	2.0			2
	GNRD23	0.1			2
	GNRD24	5.0			2
	GNRD25	10.0			2

Table 6: Comparison of corresponding radiances between two scans of the SCRIBE. Columns 4 and 5 are the radiances for the identified scans in units of erg/m sec sr cm^{-1}.

$\bar{p}$ (mb)	Bandwidth cm^{-1}	Band Center cm^{-1}	SP830V3	SP830W1
35.510	0.1	682.55	37.569	36.662
41.538		681.05	36.089	35.480
57.263		672.55	49.835	54.627
79.283		689.05	36.065	37.669
101.480		684.55	38.112	37.047
138.540		701.55	44.190	44.281
192.060		701.05	46.003	43.264
261.400		702.55	54.850	60.027
302.820		712.05	66.209	71.770
490.160		713.55	59.914	60.202
152.190	2.0	692.00	38.685	40.212
192.740		697.50	42.042	41.725
261.400		701.00	45.837	45.195
325.300		704.00	50.720	51.250
418.810		707.50	56.739	58.390
195.380	10.0	695.00	42.125	42.919
230.010		701.50	47.200	47.524
265.040		701.00	46.779	47.253
302.820		702.50	48.618	49.217

4. by the number of radiance levels assigned to each $\bar{p}$ for numerical differentiation. Seven radiances were used in general. By reducing to five, we were able to increase by two the number of $\bar{p}$ levels in each case.

Table 6 shows a comparison of the two corresponding radiance sets taken from the two successive scans, for several specific bands in the overall set. Note that each pair in this table represents two successive measurements about three minutes apart in a specific waveband. Differences between radiances within each pair are an indication of radiance noise, since the scans should see nearly the same atmospheric thermal profile. We see that at 0.1 cm^{-1} resolution, the nominal variation is of the same order as the noise estimate reported by Gallery et al. (1987), *i.e.*, of order 2 (erg/cm^2 sr sec cm^{-1}). As the bandwidth increases, we note that the differences within radiance pairs are smaller as a result of the averaging effect of the wider bands.

We have seen in the algorithm definition (Section 3) and the synthetic radiance inversions (Section 4) that a well behaved radiance profile of radiance *vs.* $\bar{p}$ is required

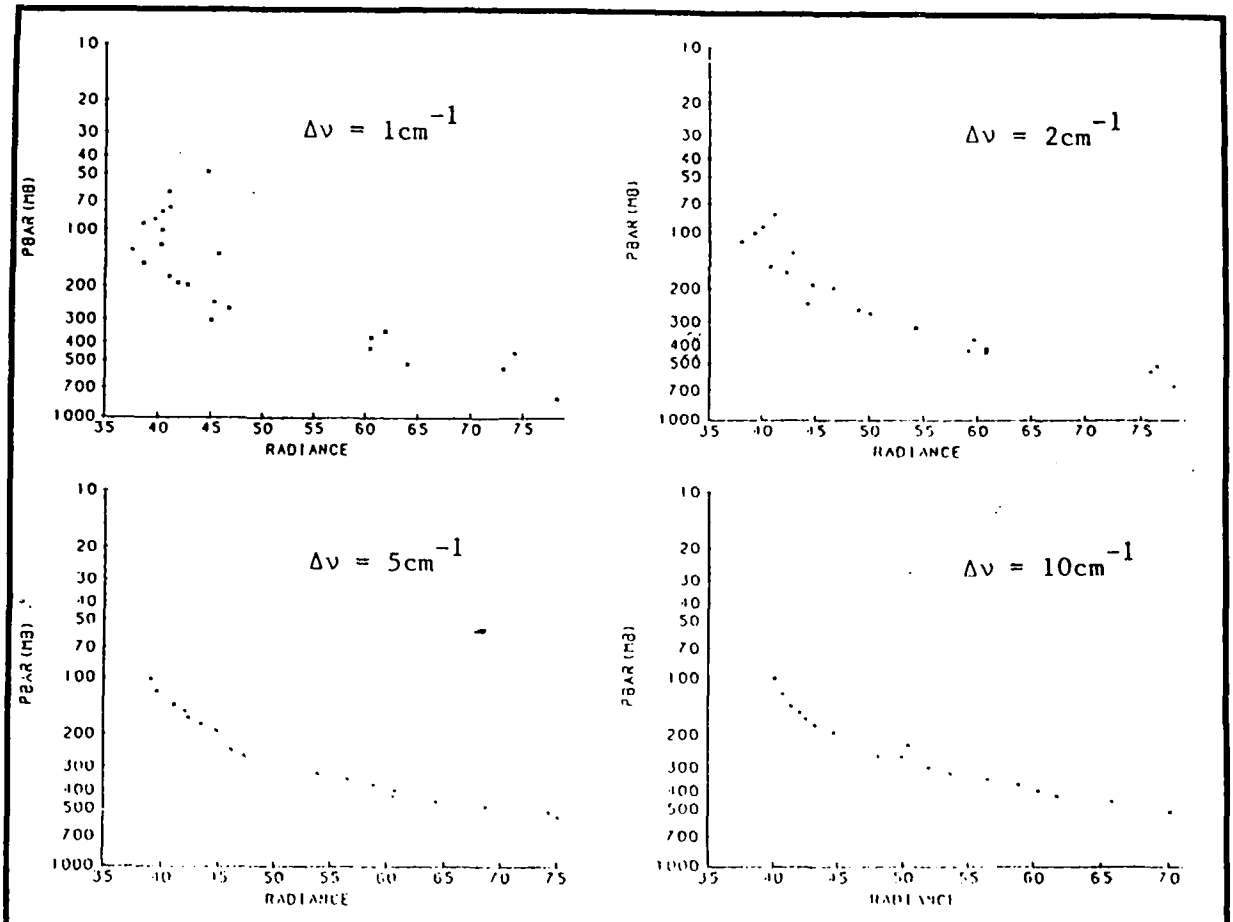

Figure 11: Radiance values *vs.* $\bar{p}$ at four values of spectral resolution for the SCRIBE radiance data selected for the inversions.

for evaluation of the derivatives. In order to evaluate the utility of the radiances we plotted the radiances within each of the first five files in Table 5. Figure 11 shows the plots. We see that a considerable scatter occurs for the fine resolution data; at the same time we see a well-behaved pattern in the radiances with a wider bandwidth.

We ascribe the scatter in the radiance data plots to the causes listed below. The relative importance of each factor cannot be evaluated quantitatively at presend. However, we have subjectively ordered the factors below (most important first) based on our understanding of the data and our experience with the FASCODE model. These are our best estimate of the related factors.

1. Noise in the radiance measurements. This is undoubtedly the primary factor. The other indicators of noise level in the SCRIBE data indicate that a large part of the scatter can be ascribed to the inherent noise.

Table 7: Results of temperature retrievals by application of the differential inversion algorithm to the SCRIBE radiances with bandwidth equal to 5.0 cm^{-1}. The symbol n_d denotes the number of derivatives used in the retrieval. Temperatures are expressed in degrees Kelvin. Pressure levels ($\bar{p}$) are in millibars.

Scan	n_d	$\bar{p}$	Computed T	T(Raob)	ΔT
SP830V1	4	192	234	218	+16
		242	209	226	-17
	3	192	236	218	+18
		242	213	226	-13
SP830W1	4	192	235	218	+17
		242	202	226	-14
	3	192	233	218	+15
		242	188	226	-26

2. Uncertainty in spectral registration of the radiance data. It is apparent from the fine structure of the radiance data in Figures 11 that very slight errors in the spectral position of the radiances would produce substantial scatter in the narrow band radiances.

3. Uncertainty in determination of $\bar{p}$ (or $\bar{\bar{p}}$), the pressure level of the peak in weight functions. The 60 level limit in FASCOD as well as numerical techniques used to locate $\bar{p}$ limit the accuracy of this parameter.

5.2.4 SCRIBE Radiance Inversion Results

The results of the differential inversion of the SCRIBE data are given in Table 7. Owing to the small number of independent $\bar{p}$ values, only two points of the temperature profile were obtained. We performed inversions for each of the two SCRIBE scans with the differential inversion series truncated at third and fourth order, thus demonstrating that the SCRIBE inversions are insensitive to the order at which the series is truncated. It can be seen that errors in the determination of temperatures were $\sim 10-20$ K, compared to radiosonde observations. The inversion of the SCRIBE data were carried out with an effective stepsize, $h \approx 0.3$, and so the errors obtained are not inconsistent with the results of the synthetic inversions (see Table 3). We note that with the small number of independent data points (4) given here and their large errors compared with radiosonde observations, that there is no significance to the trend of temperature with height shown by differential inversion of this data.

The inversions of SCRIBE data shown here are not conclusive for demonstrating the efficacy of the differential inversion algorithm. The level of accuracy of these results illus-

trates problems for the differential inversion algorithm arising from the calibration and noise level of the SCRIBE data, fundamental difficulties with finite-difference schemes in the presence of noise, and the approximation of SCRIBE weight functions by generalized exponentials. Improved techniques for differential inversions, currently under development, will control a large portion of these errors.

5.3 The TOVS Application

5.3.1 Description of the TOVS

The TIROS Operational Vertical Sounder (TOVS) consists of three instruments: (1) the High Resolution Infrared Sounder (HIRS-2), (2) the Stratospheric Sounding Unit (SSU), and (3) the Microwave Sounding Unit (MSU). In total the TOVS measures radiances in 27 channels. The band limits of the various channels and information regarding the bandwidths and peak levels of the weight functions are given in the NOAA Polar Orbiter Data User's Guide (NOAA 1983) and in Smith *et al.* (1979). Of the 27 TOVS channels, 12 channels of the HIRS-2 (1-7 and 13-17), the three SSU channels, and three of the four MSU channels respond primarily to changes in the atmospheric temperature profile.

The infrared channels of the TOVS cover fairly broad spectral bands. For Channel 1, which has the smallest bandwidth among the infrared channels, the half-power bandwidth is about 4 cm^{-1} and the one tenth-power bandwidth is about 9 cm^{-1}. The other infrared channels have half-power bandwidths of approximately 20 cm^{-1} and one tenth-power bandwidths of approximately 30 cm^{-1}. Note that in comparison to the SCRIBE data discussed in Section 5.2, the TOVS infrared data have comparatively coarse spectral resolution.

5.3.2 Selection of Data

TOVS data were provided by the National Environmental Satellite Data and Information Service (NESDIS) from the operational data processed by NESDIS in routine daily operations. The particular radiance data which we used in this study were taken from a data sample collected during the period 16-18 October 1987. The sample consisted of 15 clear column radiance sets from each of three latitude bands. The radiance data from each latitude band were accompanied by a set of transmittance profiles that were computed by NESDIS from the average temperature-moisture profile in that latitude band. These transmittances were computed by the method developed by Weinreb *et al.* (1981).

5.3.3 Differential Inversion of TOVS data

The transmittances provided by NESDIS on a grid of 40 atmospheric levels were numerically differentiated to obtain weight functions. Computation of inversion coefficients, λ_i, for large values of i, is still ill-conditioned since the evaluation of high moments of the weight function on a coarse grid is required. Therefore, we fit generalized exponential weight functions to the weight functions found from NESDIS transmittances and used those fitted weight functions to calculate λ_i values. The generalized exponential fits were obtained by first determining the maximum value of the empirical weight function based on numerical differentiation (centered divided difference) of the NESDIS transmittances and fixing this value as $\bar{p}$ in $\mathcal{P} = p/\bar{p}$ as in eq. (9). Then an m value was determined which minimized the *rms* error between the generalized exponential weight function on the grid of the NESDIS pressure levels. The fitting procedure exploits the character of the generalized exponential function as a one-parameter family of functions (*i.e.* determined by m values).

The differential inversion of TOVS data produced results significantly better than those obtained for SCRIBE. The procedure for the differential inversion of TOVS data was identical to that for the SCRIBE. Pressure levels were selected to give the most stable results (see discussion in sections 4 and 5.2.4), with a stepsize $h \approx 0.3 - 0.4$. Table 8 gives the temperature values obtained for the $2190 - 2360$ cm^{-1}, mid-latitude TOVS data. Figure 12 follows by plotting inferred temperatures against Raob temperatures for all TOVS data. The discrepancy between inferred temperatures and Raob data is on the order of $\pm 2 - 3$ degrees for points in the $\bar{p}$ grid selected in the 2190 to 2360 cm^{-1} range and $\pm 15 - 20$ degrees for points in the 668 to 748 cm^{-1} region.

For sake of completeness, we shall show explicitly the computations for one of the TOVS differential inversions. The radiance values for the first scan in Table 8 are given in Table 9. For a generalized exponential weight function with $m = 0.49$, we obtain by Romberg integration differential inversion coefficients of $\lambda_0 = 1.0$, $\lambda_1 = -0.621798$, $\lambda_2 = -0.451558$, and $\lambda_3 = 0.00438163$. Evaluating the radiance derivatives and multiplying by the differential inversion coefficients, we find,

$$B(400\text{ mb}) = 0.165079 + 0.120947 - 0.1\,.3742 - 0.000557984 = 0.11726 \text{ erg/s cm}^2 \text{ str cm}^{-1} \quad (1)$$

using terms out to third order. This result suggests that convergence is rapid, in fact, the third order term does not contribute significantly to the derived temperature. This rapid convergence implies that application of differential inversion will be computationally effective in practical applications.

We note that, within the context of very limited data, the TOVS results in the 668 to 748 cm^{-1} region are similar to the temperature differences obtained for the SCRIBE data. The difference in behavior between the wavelength regions suggests that at small inverse wavelength, small changes in radiance correspond to large changes in tempera-

Table 8: Differential inversion results for TOVS. The value of $\bar{p}$ is 400 millibars.

Latitude	Longitude	Time	Inferred Temperature	Raob Temperature	ΔT
27.2	-82.6	13:30:22	253.27	252.75	+1.52
24.3	123.8	11:12:19	255.53	256.25	-0.72
29.1	122.1	11:13:51	254.83	255.25	-0.42
14.7	120.8	23:41:12	256.00	257.16	-1.16
-14.8	-171.4	18:46:07	255.04	257.20	-2.16
-29.6	32.6	17:42:47	247.87	245.19	+2.68
-20.0	139.4	22:09:22	253.57	254.25	-0.68
27.7	-82.6	00:44:30	254.40	252.05	+2.35
23.7	154.2	09:09:21	257.02	258.86	- 1.84
26.3	-79.7	13:08:17	253.61	250.55	+3.06
23.3	-106.9	14:50:41	253.63	255.69	-1.06
24.3	153.4	21:35:20	256.88	258.45	-1.57
28.3	129.1	23:15:31	253.62	252.95	+0.67
14.9	104.9	12:29:12	256.79	258.25	-1.46

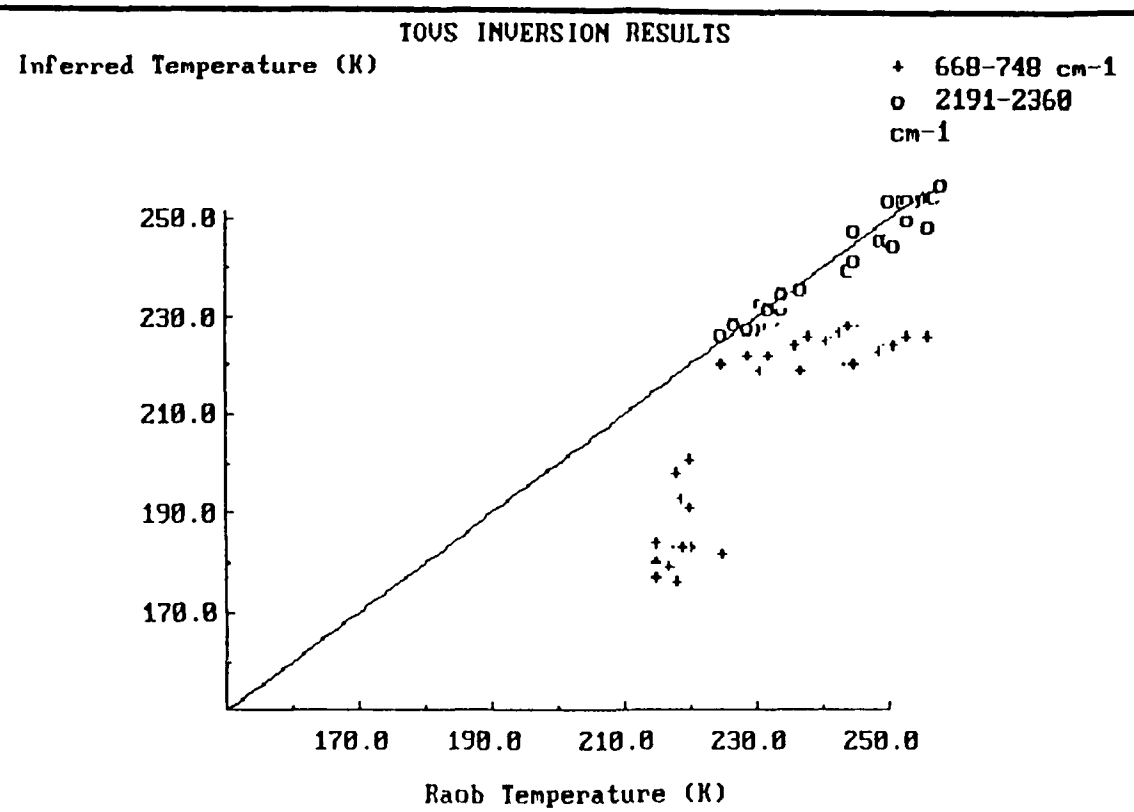

Figure 12: Temperature values obtained from application of the differential inversion algorithm to TOVS data are plotted against corresponding Raob values. Note that the low wavenumber temperatures are systematically offset from the Raob measurements.

Table 9: Radiance values for a representative TOVS scan, used for an example differential inversion computation carried out in the text. Radiances (erg/cm^2 sec sr cm^{-1}) have been normalized to channel 15.

Channel	Wavenumber (cm^{-1})	$\bar{p}$ (millibars)	Brightness Temp. (K)	Radiance (2238.45 cm^{-1})
13	2190.10	990.45	280.360	1.37306
14	2195.10	1068.75	269.410	0.860927
15	2238.45	400.00	250.230	0.344447
16	2264.95	175.08	230.950	0.117654
17	2361.70	20.00	239.470	0.193209

ture, thus temperature inference accuracy will be much more strongly affected by noise than the large inverse wavelength region of the radiance profile.

6 Conclusions

Realistic numerical experiments on synthetic radiance data have demonstrated that differential inversion techniques may be successfully employed to obtain atmospheric temperature profiles from radiance data. Applications of the differential inversion technique to SCRIBE and TOVS radiance data have shown practical problems that can be resolved by improvements in the application of the differential inversion technique and in the selection of instrumentation. At least some of these difficulties were overcome in our inversions of TOVS radiance data, and the direction of development for further improvements is clear.

When implemented in such a fashion as to require numerical differentiation of radiance data, differential inversion is sensitive to the presence of noise and to calibration errors in the radiance data. These problems limit the stepsize, h, of the calculations in logarithmic pressure space so as to control the magnitude of the relative numerical error. In application to SCRIBE data, differential inversion produced typical errors $\sim$ 20 K, and for TOVS data typical errors $\sim$ 2 K.

The problems outlined here are fundamental to any form of the differential inversion algorithm dependent upon finite-difference evaluation of derivatives. Improvements in the application of the differential inversion technique based upon insights gained from radiative transfer theory may allow us to circumvent this difficulty.

7 Recommendations

As a result of our research it is possible to make several recommendations which will allow more effective exploitation of the advantages of the differential inversion algorithm, particularly its computational efficiency, in future generations of atmospheric sounders.

1. A larger number of channels is required to evaluate the temperature profile at more heights in the atmosphere, particularly if finite difference schemes are employed (but see item 4 below).

2. Accurate calibration and high spectral resolution of the atmospheric sounding hardware will permit more accurate evaluation of numerical derivatives, with a substantial positive impact on the accuracy of the differential inversion results.

3. If a new instrument is to be designed, an investigation into the availability of channels that can be selected such that narrow weight functions corresponding to desired $\bar{p}$ values can be obtained.

4. Algorithmic techniques eliminating the requirement for evaluation of numerical derivatives in the differential inversion technique should be vigorously pursued. These theoretical developments could have the largest positive impact on the utility of the differential inversion algorithm.

8 References

Chahine, M. T. (1970): "Inverse Problems in Radiative Transfer: Determination of Atmospheric Parameters", *J. Atmos. Sci.*, **27**, 960-967.

Chahine, M. T. (1972): "A General Relaxation Method for Inverse Solution of the Full Radiative Transfer Equation", *J. Atmos. Sci.*, **29**, 741-747.

Clough, S. A., F. X. Kneizys, E. P. Shettle and G. P. Anderson (1986): "Atmospheric radiance and transmittance: FASCOD2", **Sixth Conference on Atmospheric Radiation**, Williamsburg, VA, May 1986.

Clough, S. A., F. X. Kneizys, L. S. Rothman, and W. O. Gallery (1981): Atmospheric spectral transmittance and radiance: FASCOD1B. Atmospheric Transmission, SPIE Vol. 277: 152-166. Soc. of Photo- Optical Instrumentation Engineers.

Conrath, B. J. (1972): "Vertical Resolution of Temperature Profiles Obtained from Remote Radiation Measurements", *J. Atmos. Sci.*, **29**, 1262-1271.

Gallery, W. D., D. L. Longtin and G. Tucker (1987): SCRIBE Data Validation and Analysis. Optimetrics, Inc. AFGL-TR-87-0061, ADA183538.

Gautier, D., and Revah, I. (1975): "Sounding of Planetary Atmospheres: A Fourier Analysis of the Radiative Transfer Equation", *J. Atmos. Sci.*, **32**, 881-892.

King, J. I. F. (1983): "Differential Inversion", **Ninth Conference on Aerospace and Aeronautical Meteorology**, Am. Meteorol. Soc., Boston, MA.

King, J. I. F. (1985): "Theory and Application of Differential Inversion to Remote Temperature Sensing", **Advances in Remote Sensing Retrieval Methods**, A. Deepak, H. E. Fleming, and M. T. Chahine (Eds.), A. Deepak Publishing Co.

Murcray, F. H., F. J. Murcray and D. G. Murcray (1984): "Liquid Nitrogen-Cooled Fourier Transform Spectrometer System for Measuring Atmospheric Emission at High Altitudes", *J. Atmos. Tech.*, 1(4), 351-358.

Murcray, D. G., F. H. Murcray and F. J. Murcray (1985): " Measurements of Atmospheric Emission at High Spectral Resolution", *J. Meteor. Soc. of Japan*, **63**(2), 320-324.

NOAA (1983): "NOAA Polar Orbiter Data Users' Guide", National Climatic Data Center, National Oceanic and Atmospheric Administration.

Rothman, L. S. (1981): "AFGL Atmospheric absorption line parameters compilation:

1980 version", *Appl. Opt.*, **20**, 791.

Sakai, H. and Vanasse, G. (1984): "SCRIBE Data of October 23, 1983 Flight", AFGL-TR-84-0208, Air Force Geophysics Laboratory, ADA154864.

Sakai, H., 1985: Processing of SCRIBE Data. AFGL-TR-85-0279. University of Massachusetts, ADA165226.

Smith, H. J. P., Dube, D. J.,Gardner, M. E.,Clough, S. A.,Kneizys, F. X., and Rothman, L. S. (1978): "FASCODE - Fast Atmospheric Signature Code (Spectral Transmittance and Radiance)", AFGL-TR-78-0081, Air Force Geophysics Laboratory, ADA057506.

Smith W. L. (1970): "Iterative Solution of the Radiative Transfer Equation for the Temperature and Absorbing Gas Profile of an Atmosphere", *Appl. Opt.*, **9**, 1993-1999.

Smith, W. L., Woolf, H. M., Hayden, C. M., Wark, D. Q., and McMillin, L. M. (1979): "The TIROS-N Operational Vertical Sounder", *Bull. Amer. Meteor. Soc.*, **60**, 1177-1187.

Twomey, S. (1970): "Information Content and Indirect Sensing Measurements",*J. Atmos. Sci.*, **27**, 515-518.

Vanasse, G. (1981): "Stratospheric Cryogenic Interferometric Balloon Experiment", AFGL-TR-81-0048, Air Force Geophysics Laboratory, ADA100218.

Weinreb, M. P., Fleming, H. E., McMillin, L. M., and Neuendorffer, A. C. (1981): "Transmittances for the TIROS Operational Vertical Sounder", NOAA Technical Report NESS 85, National Oceanic and Atmospheric Administration.

Widder, D. V. (1971): **An Introduction to Transform Theory**, Academic Press, New York.

Yeh, H-Y. M., Vonder Haar, T. H., and Liou, K-N. (1985): "Cloud Parameters and Temperature Profile Retrieval from Infrared Sounder Data", *J. Atmos. Sci.*, **42**, 2360-2370.

A SCRIBE Weight Functions from TOVS Transmittances

Initially weight functions used for differential inversion were computed directly by numerical differentiation of a transmittance profile computed using FASCOD2. A pressure grid of 60 levels was used, which is the finest grid supported by FASCOD2. The weight functions were computed by a standard centered divided difference scheme, with forward and backward divided difference calculations performed at the edge of the grid, as required.

In the figures, a randomly selected sample of weight functions computed from FASCOD2 transmittances is shown both with pressure and logarithm (base 10) of pressure as independent variable. The plot of weight function against logarithm of pressure is particularly useful for illustrating the problems with the weight functions we have found here, which are most important at low pressures. Although numerical inaccuracies of the FASCODE transmittances are not apparent in plots of the transmittance function, tney are significant for the weight functions, because numerical differentiation effectively amplifies relative numerical error. The result is that the weight functions are no longer smooth, but exhibit substantial fluctuations between adjacent points over the low pressure range of the pressure grid.

Application of the differential inversion algorithm assumes that the weight functions must be reasonably smooth functions, and in fact this is an important requirement for the numerical stability of the inversion algorithm. A portion of the difficulty may be seen by considering the evaluation of the λ coefficients for the series in equation (8). Determination of these coefficients requires the evaluation of moments of the weight function. Applying equation (6),

$$\lambda_k = \frac{1}{k!}\{\frac{d^k}{ds^k}[1/w(-s)]|_{s=0}\} \qquad (A1)$$

which implies

$$\lambda_k = \frac{1}{k!}\{\frac{d^k}{ds^k}[\frac{1}{\int_0^\infty p^{-s}\mathcal{W}(p)dp/p}]|_{s=0}\} \qquad (A2)$$

and so evaluation of λ_k involves computation of the $k-1$th and lower moments of the weight function. For large values of k, calculation of moments, particularly emphasizes the importance of any inaccuracies in the "wings" of the weight function, *i.e.* at the low pressure and high pressure and high pressure ends of the pressure grid. Therefore, the calculation of λ coefficients from FASCODE transmittances is unreliable.

To circumvent this problem for application of differential inversion to the SCRIBE data, we fitted generalized exponential weight functions to the weight functions obtained by numerical differentiation of the FASCOD2 transmittances. Values of m were determined to three significant figures by minimization of *rms* errors on the FASCODE pressure grid.

Using this m value, λ coefficients were found for the inversion by taking appropriate moments of the generalized exponential weight functions.

Inspection of the graphs of the weight functions shows that the problems with the FASCOD2 transmittances principally arise at the edge of the pressure grid and might be attributed to some sort of edge effect in the FASCOD2 computations of the transmittances. The fluctuations in the weight functions are not attributable to use of forward or backward divided differences at the edge of the grid for computation of the weight function (as opposed to centered divided differences) since the fluctuations occur up to 5 or 6 grid points interior to the edge of the pressure grid. The relative accuracy of computation of FASCODE transmittances will have to be increased by approximately an order of magnitude in order to achieve the degree of smoothness required to directly determine λ coefficients from FASCODE transmittances.

Some advantage may be gained by smoothing the FASCODE transmittances to the actual accuracy of the transmittances. This smoothing would alleviate some of the problems arising from the fluctuations in the transmittance profiles at the low pressure end of the pressure grid. This same smoothing effect is probably inherent to the NOAA statistical transmittance model.

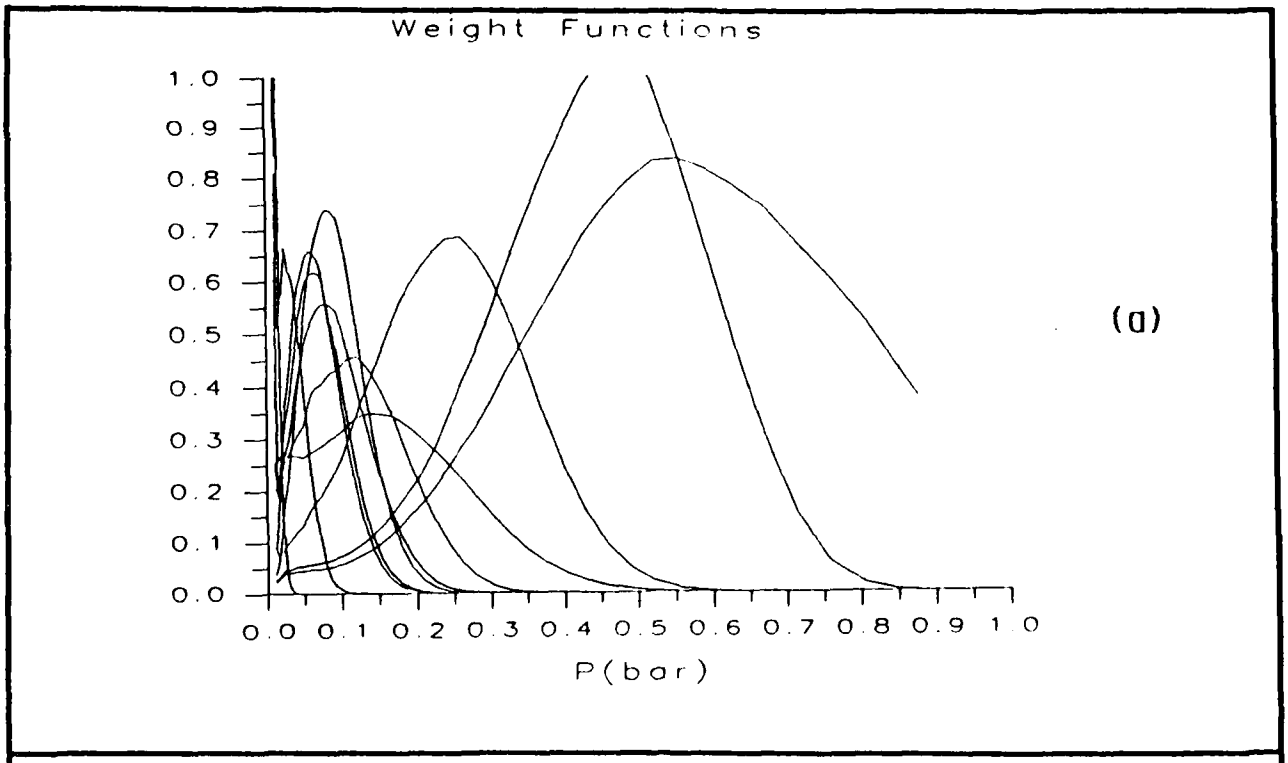

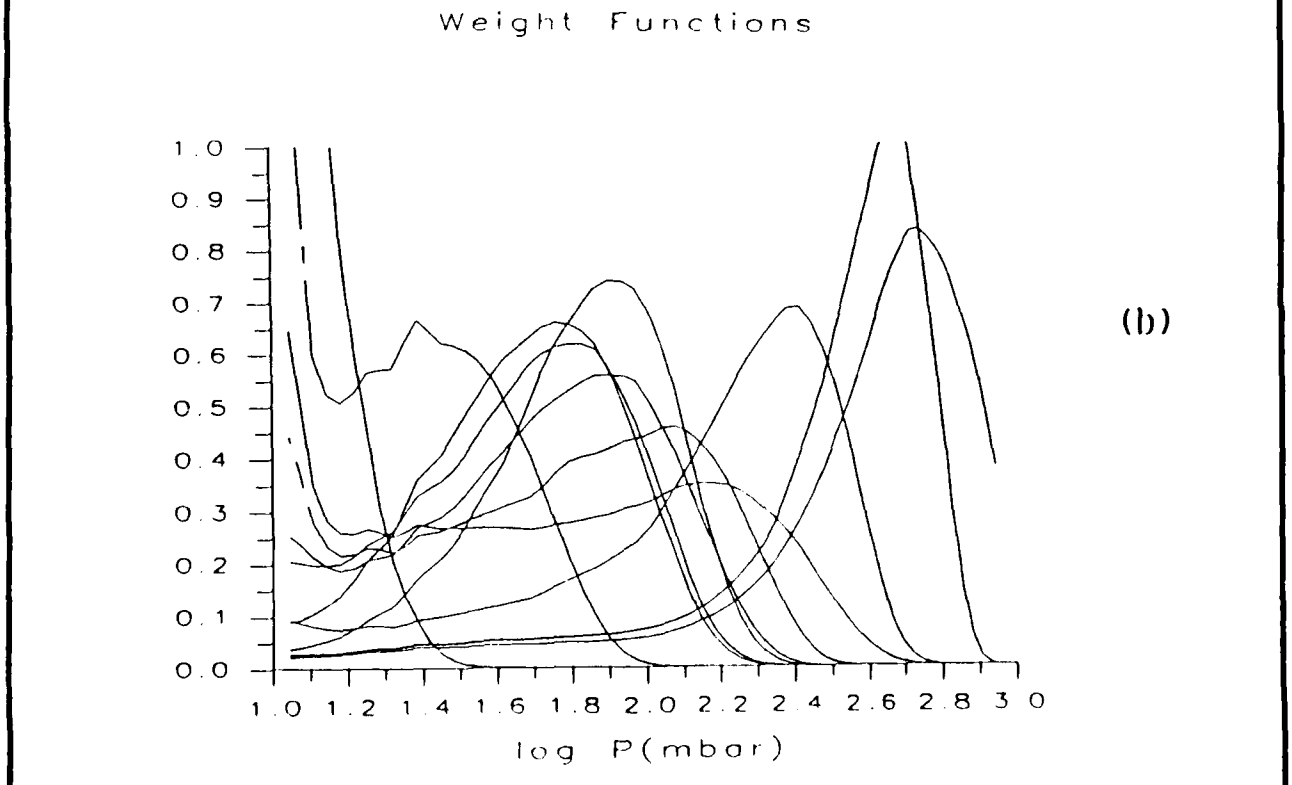

Figure A1: Randomly selected weight functions determined by numerical differentiation of FASCODE transmittances. In (a) the independent variable is the atmospheric pressure in bars, while in (b) it is the $\log_{10}$ of the pressure in millibars.